63-3-2

TRG

INCORPORATED

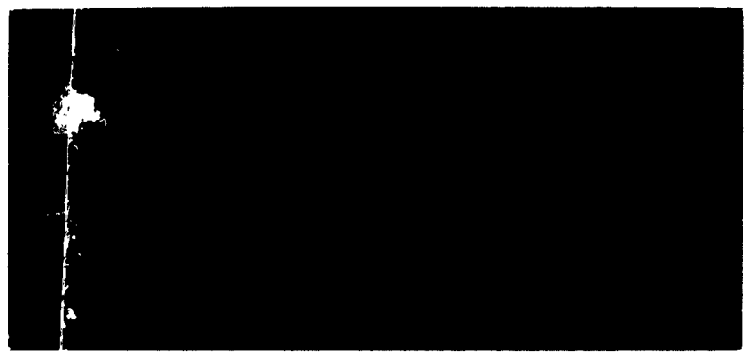

TECHNICAL RESEARCH GROUP
2 AERIAL WAY • SYOSSET, NEW YORK

Submitted by:

TRG, Incorporated
2 Aerial Way
Syosset, New York

CAVITY SHAPE AND DRAG IN VENTILATED FLOW; THEORY AND EXPERIMENT

Author: P. Thomsen
Peter Thomsen

Approved: Hanan Rubin
Hanan Rubin

Submitted to:

Scientific Officer
Head, Fluid Dynamics Branch,
Mathematical Sciences Division
Office of Naval Research
Washington, D.C.

February 1963

TABLE OF CONTENTS

LIST OF ILLUSTRATIONS

LIST OF ILLUSTRATIONS (Cont'd)

ACKNOWLEDGMENT

We are indebted to Prof. S. Karp for suggesting the principal idea in the three-dimensional analysis; and to Prof. S. Karp and Dr. J. Kotik for a number of consultations.

1. INTRODUCTION

In a previous report, TRG-156-SR-1, the two-dimensional cavity theory was applied to ventilated flow around surface-piercing struts. The strut cross-section shapes considered were rectangular, circular, triangular, and parabolic. The theoretical results obtained for cavity length and cavity drag were compared with experimentally obtained values for a series of cases. The results indicated that two-dimensional theory is inadequate for length prediction; however, the results obtained for cavity drag showed substantial agreement.

The present report offers a three-dimensional analytic approach to predicting cavity length. It also compares the theoretical results with length measurements that were made in cavity side photos published by B. Perry [1] and A.D. Hay [2].

In our analysis of the Hay experiments special emphasis was placed on the different flow states that can be observed with increasing speed. For instance, at high speed, the strut cavity is sealed off from the atmosphere by the surface flow, causing a change in flow state.

Further comparisons are carried out between experimental drag and theoretical drag, calculated on the two-dimensional basis.

The results obtained for cavity length can be used as a guide for developing further the theory of cavity shape. Such theory may form the basis for a three-dimensional drag analysis. Furthermore, information about cavity shape may be applicable to the design of a strut-hydrofoil-system. The most practical way of

providing the ventilation required by a hydrofoil cavity is to have the strut cavity open to atmospheric air, and to have it reach down to the strut-base for supercavitating foils or to the strut-and foil-base for base-ventilated foils.

2. THREE-DIMENSIONAL ANALYTIC APPROACH TO CAVITY LENGTH

We consider a cavity behind a surface-piercing strut, where the cavity is open to atmospheric air and reaches down to the base of the strut. The strut base is in z = -H (H = strut submergence). The xy-plane of the coordinate system is in the undisturbed free surface, positive x being opposite to the incident uniform flow of speed U. The vertical coordinate z is positive upwards. Regarding strut geometry, we only consider strut submergence H; we do not account for the lateral dimension d (strutbeam). The cavity length at z = 0 is denoted by L.

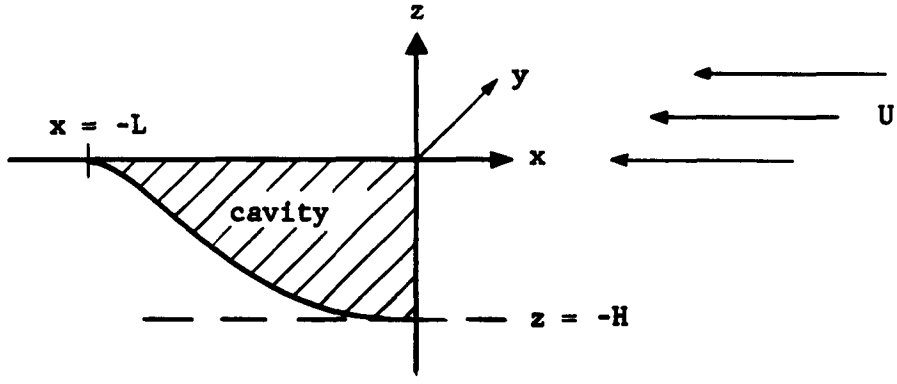

Figure 1: Coordinate system and notation for ventilated cavity.

The flow is considered as potential flow, thus the velocity potential is

(1) $$\Phi = -Ux + \phi \quad .$$

Here ϕ is the potential of the disturbance velocities. By Bernoulli's equation, the dynamic boundary condition that the pressure in the cavity walls equals the atmospheric pressure is - neglecting ϕ_x^2, ϕ_y^2, ϕ_z^2 - given by

(2) $$\phi_x = \frac{gz}{U} \quad ,$$

where g is the acceleration due to gravitation. Assuming slender cavities we apply (2) at y = o in the cavity region. By integrating (2) with respect to x, we then obtain the potential ϕ, applicable to y = o in the cavity region, namely

(3) $$\phi(x, o, z) = \frac{gzx}{U} + h(z) \quad .$$

Here h(z) is an unknown, z-dependent constant of integration. The ϕ_z-velocity is then

(4) $$\phi_z(x, o, z) = \frac{gx}{U} + h'(z)$$

in the cavity region; $h'(z)$ represents $\phi_z(o, o, z)$. Eq. (4) can also be obtained directly from (2), if we use the condition of irrotationality

(5) $$\phi_{xz} - \phi_{zx} = 0 \quad ,$$

which in conjunction with (2) yields

(6) $$\phi_{xz} = \phi_{zx} = \frac{g}{U} \quad .$$

Applying this in y = o and integrating ϕ_{zx} with respect to x, Eq. (4) is obtained. Assuming the derivatives of ϕ to be continuous at the point (-L, o, o), we apply at this point the free surface boundary condition

(7) $$\left(\phi_{xx} + \frac{g}{U^2}\phi_z\right)_{z=o} = 0 \quad .$$

However, (2) implies that

(8) $$\phi_{xx} = 0$$

and thus

(9) $$\phi_z = 0 \quad .$$

Hence, we obtain from (4)

(10) $$\phi_z(-L, o, o) = -\frac{gL}{U} + h'(o) = 0 \quad .$$

From (10) we conclude that

$$h'(0) = \frac{gL}{U} \quad . \tag{11}$$

In this way h'(z) is determined for z = 0.

We apply now, instead of Eq. (4), the approximation

$$\phi_z(x,o,z) \approx \frac{gx}{U} + \frac{gL}{U} \quad , \tag{12}$$

replacing h'(z) by h'(0). The reasoning is that relevant experiments show an approximately constant upward velocity on the front of the strut at depths located between the tip end region and the free surface region. Certainly, it is incorrect to apply h'(0) for this velocity; (12) has to be looked upon as an assumption.

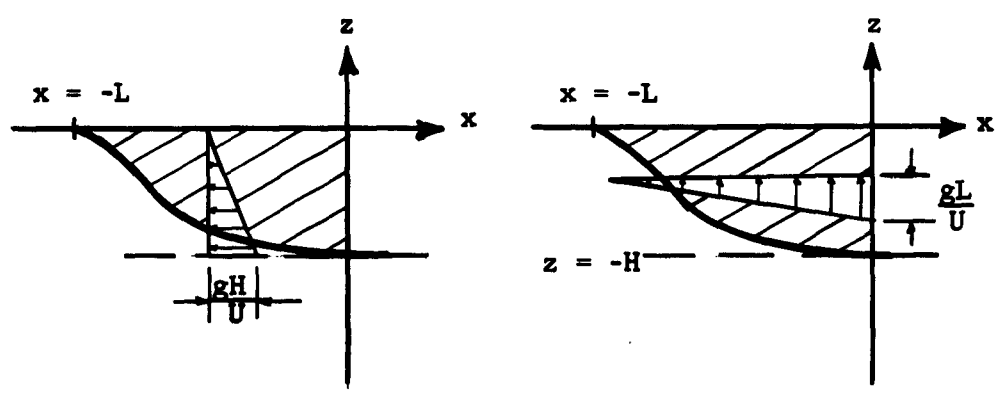

Figure 2:

Disturbance velocity $\phi_x(x,o,z)$; according to Eq. (2) - it is independent of x.

Disturbance velocity $\phi_z(x,o,z)$; according to Eq. (12) - it is independent of z.

(Velocities apply to the cavity region which is hatched.)

We now consider the cavity shape. The cavity walls are composed of streamlines, and the cavity rear is also considered as a streamline. The differential equation of this rear streamline is

$$\frac{dx_r}{dz_r} = \frac{(\phi_x)_r}{(\phi_z)_r} = \frac{gz_r - U^2}{gx_r + gL} \quad . \tag{13}$$

The integration

$$\int_{-H}^{z_r} (gz_r' - U^2)\,dz_r' = \int_{o}^{x_r} (gx_r' + gL)\,dx_r' \tag{14}$$

leads to

$$x_r = \sqrt{z_r^2 - 2z_r \frac{U^2}{g}} - L \quad . \tag{15}$$

Considering that $x_r = 0$ for $z_r = -H$ we find

$$L = \sqrt{H^2 + \frac{2HU^2}{g}} \quad . \tag{16}$$

Thus we have

$$x_r = \sqrt{z_r^2 - 2z_r \frac{U^2}{g}} - \sqrt{H^2 + \frac{2HU^2}{g}} \quad . \tag{17}$$

The cavity length

$$\ell = |x_r| \tag{18}$$

can be obtained from (17) at any depth z_r. The final result - nondimensionally and dropping the subscript r - is

$$(19) \qquad \frac{\ell(z)}{H} = \left| \sqrt{\left(\frac{z}{H}\right)^2 - 2\left(\frac{z}{H}\right)\frac{U^2}{gH}} - \sqrt{1 + 2\frac{U^2}{gH}} \right| .$$

Here $\frac{U^2}{gh}$ appears as a parameter; for $\frac{U^2}{gH}$ = const. and any submergence H the rear shapes given by Eq. (19) are geometrically similar as the submergence H is varied. The parameter $\frac{U^2}{gH}$ is the square of the Froude number f (based on length H), where f is given by

$$(20) \qquad f = \frac{U}{\sqrt{gH}} .$$

It is also the reciprocal of half the nominal base cavitation number

$$(21) \qquad \sigma(-H) = \frac{2gH}{U^2} .$$

3. COMPARISON WITH EXPERIMENTAL CAVITY LENGTHS

a. Different Flow States

Observed ventilated flows in real fluids depend on the three parameters $\frac{gH}{U^2}$, $\frac{d}{H}$, and $\frac{Ud}{\nu}$. The speed parameter $\frac{gH}{U^2}$, related to the nominal cavitation number of the incident flow at depth H and also to the cited Froude number of the "strut-incident flow" system, governs the cavitation mechanism and the occurring surface waves. The strut beam to submergence ratio, $\frac{d}{H}$, essentially influences the disturbance velocities generated by the strut. (The strut beam d in case of circular struts is the diameter; in case of rectangular struts it is the width). The Reynolds number too, $\frac{Ud}{\nu} = Re$, representing the ratio of mass to viscosity forces in the flow (where ν denotes kinematic viscosity), influences the field of disturbance velocities.

Experiments show three possible states of cavitation and ventilation: the cavitation inception and pre-base ventilation state, the base ventilation state, and the post-base ventilation state. In the inception and pre-base ventilation state, the ventilated cavity is building up behind the strut with increasing speed, reaching down to a depth somewhere above the strut base. In the base ventilation state, the bottom of the ventilated cavity springs from the strut-base. In the post-base ventilation state, the cavity behind the strut is sealed off at the free surface by the flow, its contents being vapor (see Fig. 3).

The boundaries between these states are plotted for struts of circular cross-section in Fig. 4. Fig. 4 was obtained by analyzing the experiments of A.D. Hay [2]. These experiments were run in a systematic and extensive program on struts of circular section-shape. Fig. 4 shows that for fixed $\frac{d}{H}$, with decreasing $\frac{gH}{U^2}$ base ventilation is reached at a $\frac{gH}{U^2}$ of the order of 0.3 - where the actual magnitude depends on Reynolds number $Re = \frac{Ud}{\nu}$ - and that the post-base ventilation state is reached at some lower value of $\frac{gH}{U^2}$. The effect of Re for this latter boundary is appreciably smaller. The $\frac{gH}{U^2}$ at this boundary is about 0.005 for $\frac{d}{H}$ of about 1 or 1/2 but approaches 0.3 as $\frac{d}{H}$ tends to 0. This means that, for a comparatively deep strut, base ventilation cannot be attained at all.

The theoretical approach for the determination of cavity lengths in the previous section was concerned with the base ventilation state. Here the analysis could be based on the fixed depth $z = -H$ where the cavity rear streamline starts. Certainly the analysis of Section 2 holds for cavity depths $h < H$, that is for the pre-base ventilation state. But here h is theoretically not known; one certainly could use experimental values of h.

b. <u>Comparisons Not Accounting for the Reynolds Number in Experiments</u>

Fig. 5 shows a comparison of experimental cavity lengths with 2D-theoretical and 3D-theoretical results. The experiments are those conducted by Perry [1] on a strut of rectangular cross-section. The strut has a fixed submergence (H=8"), fixed width (d=1/8") and

various speeds (U = 10, 12, 15 fps). The parameter $\frac{d}{H}$ is $\frac{1}{64}$; the parameter $\frac{gH}{U^2}$ is 0.095, 0.148, and 0.215. Reynolds number as occurring in the experiments is not taken into account.

The improvement obtained here by use of 3D-theory is obvious: the 3D-theoretical lengths in z = 0 are finite, the 3D-theoretical lengths in 0 > z > -H agree better with experiment. Quantitative agreement is good in the case of high speed (low $\frac{gH}{U^2}$) but deteriorates with decreasing speed ($\frac{gH}{U^2}$ getting larger). Considering the limitations of the theoretical approach, we did not expect good quantitative agreement for all combinations of parameters $\frac{d}{H}$, $\frac{gH}{U^2}$ and Re. The theory can be interpreted as developed for $\frac{d}{H} = 0$ (no lateral dimension), Re = ∞ (no viscosity). Certain z-velocities were assumed in the cavity rear streamline.

We next try to find the ranges of parameters $\frac{d}{H}$ and $\frac{gH}{U^2}$ where best agreement can be found with the Hay experiments [2].*

First we ignore the effect of the Reynolds number in the experiments. We consider cases where $\frac{d}{H}$ = const., $\frac{gH}{U^2}$ = variable. See:

Fig. 6 for $\frac{d}{H} = \frac{1}{16}$, based on d = $\frac{1''}{8}$, H = 2" ,

Fig. 7 for $\frac{d}{H} = \frac{1}{16}$, based on d = $\frac{1''}{4}$, H = 4" ,

---

* To understand the parameter variation carried out in the following, the reader should look up Fig. 4 of this paper and see that with the variation of $\frac{gH}{U^2}$ (when $\frac{d}{H}$ is fixed) we horizontally cross the phase of base ventilation and that with the variation of $\frac{d}{H}$ (when $\frac{gH}{U^2}$ is fixed) we vertically cross the phase of base ventilation in Fig. 4.

Fig. 8 for $\frac{d}{H} = \frac{1}{2}$, based on $d = \frac{1''}{2}$, $H = 1''$,

Fig. 9 for $\frac{d}{H} = 1$, based on $d = 2''$, $H = 2''$.

Each figure shows a series of cases for decreasing $\frac{gH}{U^2}$. (The Reynolds number applicable to the individual experiment is indicated for informative purposes.) In each figure length increases as $\frac{gH}{U^2}$ approaches 0 from both experiment and theory. However, the rate of increase in the experiments is always higher than that in theory.

Thus, agreement is possible if at the transition from the pre-base ventilation to the base ventilation state $\ell_{exp.}$ is predominantly less or equal to $\ell_{theor.}$ on the rear line. Thus, in Fig. 6 (at $\frac{gH}{U^2} \approx 0.18$) and in Fig. 7 (at $\frac{gH}{U^2} \approx 0.085$) we find a $\frac{gH}{U^2}$ for which some agreement can be observed; this is not true in Fig. 8 and Fig. 9.

Still ignoring Re in the experiments, we next consider cases where $\frac{gH}{U^2}$ = const., $\frac{d}{H}$ = variable. See

Fig. 10 for $\frac{gH}{U^2} = 0.214$,

Fig. 11 for $\frac{gH}{U^2} = 0.084$.

Each figure shows a series of cases for increasing $\frac{d}{H}$. (The Reynolds number applicable to each experiment is indicated.) In these series, the experimental lengths increase with increasing $\frac{d}{H}$ - up to somewhere around $\frac{d}{H} = \frac{1}{4}$ or $\frac{d}{H} = \frac{1}{2}$. With $\frac{d}{H}$ approaching 1 they no longer

change monotonically and they vary at lower rates. The theoretical lengths, however, are always constant (as $\frac{gH}{U^2}$) since $\frac{d}{H}$ was not included in the theory. Thus, agreement is found somewhere in the range $0 < \frac{d}{H} < 1$ if, for the chosen $\frac{gH}{U^2}$ and small $\frac{d}{H}$, $\ell_{exp.}$ is predominantly equal or less than $\ell_{theor.}$ over the rear line, and only then. Thus, in Fig. 10 we find at $\frac{d}{H} \approx \frac{1}{3}$ some agreement but not in the series of Fig. 11.

Summarizing now Figs. 6 through 11 we have the following: For small $\frac{d}{H}$ ($\frac{d}{H} = \frac{1}{16}$, $\frac{1}{8}$) fair agreement can be found. For higher $\frac{d}{H}$ agreement is not possible. At the transition from the pre-base ventilation to the base ventilation state for such $\frac{d}{H}$ $\ell_{exp.} > \ell_{theor.}$ over the rear line and both the approach of $\frac{gH}{U^2}$ to 0 and the approach of $\frac{d}{H}$ to 1 tend to increase $\ell_{exp.}$ over $\ell_{theor.}$. The influence of $\frac{d}{H}$ is essential. The change in lateral dimension d, however, affects also the Reynolds number $Re = \frac{Ud}{\nu}$. The theory does not account for the effects of $\frac{d}{H}$ and Re.

Before taking Re into account when selecting the experiments, we wish to draw attention to the relation with the Perry series (Fig. 5), where our comparisons did originate. There, for $\frac{d}{H} = \frac{1}{64}$, the best agreement is at $\frac{gH}{U^2} = 0.095$. The corresponding series in the Hay experiments is in Fig. 6 and Fig. 7. Here we find $\frac{d}{H} = \frac{1}{16}$ and best agreement at $\frac{gH}{U^2} \approx 0.18$ (Fig. 6) and at $\frac{gH}{U^2} \approx 0.085$ (Fig. 7). Thus, we find a shift in $\frac{d}{H}$ and a possible shift in $\frac{gH}{U^2}$. We do not find a direct agreement with the Perry case.

The shift in $\frac{d}{H}$ is certainly connected with the difference in shape (rectangular vs. circular). The point is that in the experiments with the circular struts, there is no base ventilation at all for $\frac{d}{H} = \frac{1}{64}$; for $\frac{d}{H} = \frac{1}{32}$ base ventilation exists over a comparatively narrow range of $\frac{gH}{U^2}$ (see Fig. 4 for $\frac{d}{H} = \frac{1}{64}$ and $\frac{d}{H} = \frac{1}{32}$). Thus the Hay series corresponding to that of Perry is found at a higher $\frac{d}{H}$ only. Here base-ventilation occurs over a $\frac{gH}{U^2}$-range of comparable width.

c. Comparisons Accounting for Reynolds Number in the Experiments

In a series of additional comparisons we took account of the Reynolds number, $Re = \frac{Ud}{\nu}$, with $\nu = 1.58 \cdot 10^{-3}$ sq. inch/sec at 68°F, the average temperature of the experiments. We found that the basic influence of the parameters $\frac{gH}{U^2}$ and $\frac{d}{H}$ is not changed when Re $\approx$ constant in the experiments. With $\frac{gH}{U^2}$ approaching 0 the experimental cavity length increased and with $\frac{d}{H}$ approaching 1 it increased, as seen earlier.

We were led to this result by comparing cases where

$\frac{d}{H}$ = const., Re $\approx$ const., $\frac{gH}{U^2}$ = variable ..... series (a) ,

$\frac{gH}{U^2}$ = const., Re $\approx$ const., $\frac{d}{H}$ = variable ..... series (b) .

The above results were obtained at several constant Re numbers. The actual numerical value of each Re was

for the series (a) between $4.9 \cdot 10^3$ and $9.4 \cdot 10^4$,

for the series (b) between $0.8 \cdot 10^4$ and $8.7 \cdot 10^4$.

We did not show a comparison of series (a) and (b). Having no valid theory, we have no basis to discuss the modifications brought about by the effect of Reynolds number.

We do show, however, the effect of Re in the following comparisons with

$$\frac{d}{H} = \text{const.}, \qquad \frac{gH}{U^2} = \text{const.}, \qquad \text{Re} = \text{variable} \ldots\ldots \text{series (c)}$$

in Fig. 12. Fig. 12 in particular holds for

$$\frac{d}{H} = \frac{1}{8}, \quad \frac{gH}{U^2} \approx 0.084, \quad 1.08 \cdot 10^4 \leq \text{Re} \leq 2.45 \cdot 10^5 .$$

The result is that with increasing Re the experimental cavity length increases. This trend was also observed for a number of additional combinations, for example for

$$\frac{d}{H} = \frac{1}{4}, \quad \frac{gH}{U^2} \approx 0.107, \quad 1.08 \cdot 10^4 \leq \text{Re} \leq 8.65 \cdot 10^4 ,$$

$$\frac{d}{H} = \frac{1}{2}, \quad \frac{gH}{U^2} \approx 0.107, \quad 2.16 \cdot 10^4 \leq \text{Re} \leq 1.73 \cdot 10^5 ,$$

$$\frac{d}{H} = \frac{1}{16}, \quad \frac{gH}{U^2} \approx 0.214, \quad 5.3 \cdot 10^3 \leq \text{Re} \leq 1.53 \cdot 10^4 ,$$

$$\frac{d}{H} = \frac{1}{8}, \quad \frac{gH}{U^2} \approx 0.214, \quad 4.35 \cdot 10^3 \leq \text{Re} \leq 3.07 \cdot 10^4 .$$

But the influence was not as strong in other observed combinations. Whatever the proper dependence may be, it is evident that the influence of Re in the case of the circular struts for certain combinations of

parameters $\frac{gH}{U^2}$, $\frac{d}{H}$ and Re is appreciable. The effect of Re on the transition from the pre-base ventilation state to the base ventilation state was shown numerically in Fig. 4.

4. COMPARISON OF THEORETICAL CAVITY DRAG IN TWO-DIMENSIONAL THEORY WITH EXPERIMENTAL DRAG

Ventilated flow in two-dimensional theory is treated in a system of plane horizontal flow layers. If U, d, and the section shape are variable over depth z, the cavity drag on a vertical strut is computed by

$$F = \frac{\rho}{2} \int_{-h}^{0} U^2(z) d(z)\ c_D(z) dz \tag{22}$$

with ρ the mass density, d the lateral dimension of strut section, c_D the drag coefficient of section and $h \leq H$ cavity depth on the strut. The z-dependence in c_D actually is the dependence on the cavitation number $\sigma(z)$; for small σ

$$c_D(\sigma) \sim c_D(0)\ [1 + \sigma] \quad , \tag{23}$$

where σ is the nominal cavitation number of the incident flow

$$\sigma(z) = \frac{2g|z|}{U^2} \quad . \tag{24}$$

The $c_D(0)$ coefficient is known for a number of strut section shapes. (circular: $c_D(0) = 0.5$; rectangular: $c_D(0) = 0.88$; etc.) For constant U, d and constant section-shape and for small σ Eq. (22) reduces to

$$F \backsim c_D(0) \left[\frac{\rho}{2} U^2 + \frac{1}{2} \gamma h \right] d\ h \quad , \quad \gamma = g\rho \ . \tag{25}$$

We compare this theoretical cavity drag with the experimental strut drag of Hay [2]. This is presented in Figures 13 through 19. In these figures the experimental drag curves, the transitions between the different flow states and the theoretical strut cavity drag for the base ventilation state are given.

In the pre-base ventilation state, the experimental drag contains an appreciable friction drag. We cannot separate it from the cavity drag. This is the reason why we give no comparisons for the pre-base ventilation state. (The fact that in this state h is theoretically unknown would be no obstacle. It could be taken from the cavity side photos in [2] for all cases.)

In the base ventilation state, the experimental drag still contains a friction drag. Its contribution is also unknown, but it is considered small in the prevalent case of a circular strut cross-section. (For a confirmation of theory, the experimental values always should be slightly larger than the theoretical.)

For the base ventilation state the agreement between the experimental and theoretical drag is fairly good. Of the 13 series investigated, 10 series show discrepancies of 10% or less from the experimental value. Two series contain a discrepancy of about 13%; one - see Fig. 17 - displays a 33% difference.

The good agreement in the large majority of cases is surprising, since the nominal cavitation number in the flow layers of the two-dimensional model range from zero (at $z = 0$) to 0.6 (at $z = -H$). (We know definitely that the number is 0.6 since we

found the transition from the pre-base ventilation state to the base ventilation state at $\frac{gH}{U^2} \approx 0.3$ - see Fig. 4.) Equation (25), however, is based on the assumption of small σ. The good agreement is a fact. However, we do not know the meaning of the 33% difference in Fig. 17. Further comparisons similar to those carried out in this report should be investigated.

We conclude this section with an observation on the experimental strut drag at the transition from the base ventilation state to the post-base ventilation state. In this transition, the strut drag possibly jumps discontinuously to a higher level (see Figs. 15, 16) or starts increasing (with speed increasing) at a steeper gradient (see Fig. 14). This is the reason why in a low-drag-system the post-base ventilation state is problematic.

The physical reason for the discontinuous behavior of drag is most likely, that the pressure in the closed cavity is due to vapor. Representing an under-pressure in the strut rear - reference-pressure is the atmospheric pressure - it acts as a drag increment.

5. RESULTS

Cavity Lengths:

The three-dimensional theoretical analysis of cavity lengths took account of the speed parameter $\frac{gH}{U^2}$ only. The parameters $\frac{d}{H}$ and Re were not considered. We obtained fairly good agreement with experimental lengths for small $\frac{d}{H}$ at some $\frac{gH}{U^2}$ in the base ventilation-flow state. On the other hand, the theoretical lengths on the basis of the two-dimensional cavity theory do not agree with experiment.

The discrepancies between the 3D-theoretical length and the experimental length as obtained for the majority of parameter combinations were investigated. It was found that the influence of $\frac{gH}{U^2}$ as given by the theory is too weak compared with the influence of $\frac{gH}{U^2}$ from the experiment. The influence of the theoretically ignored parameter $\frac{d}{H}$ was found to be essential as is also the influence of the Reynolds number $Re = \frac{dU}{\nu}$ in some ranges.

With these results, a basis is given for possible further development of cavity shape theory in ventilated flow. There seems to be a guide now on how to include $\frac{gH}{U^2}$ and $\frac{d}{H}$.

The information about the different states of flow as obtained from our analysis of Hay's experiments seems to have direct application. Designers shsould obtain experimental graphs of the kind of our Fig. 4 for struts of practical cross-section. This will serve

(a) to compare the intended operating range of their system with the occurring base ventilation range,

(b) to stay away from the "sealing off" effect in the flow and the different, cavitated flow thereafter.

Cavity drag:

The agreement between the experimental and theoretical cavity drag determined on the two-dimensional basis is fairly good. In the majority of cases considered the difference is of the order of 10%.

However, we have no final result as to the degree of agreement since higher differences also occurred in the comparisons.

The strut drag (cavity drag) with higher speeds reaches comparatively high values once the strut cavity is sealed off from the atmosphere. This behavior was shown in the experiments used in this study.

6. Conclusions, Recommendations

In our opinion there are two main practical applications of ventilated flow theory:

1) the prediction of cavity drag force,

2) the prediction of the various flow states.

The prediction of cavity shape may be important in some special cases and this may be a third application.

We suggest additional work to establish theoretical and experimental data that further meet practical requirements.

Further comparisons should be carried out between experimental and 2D-theoretical drag on struts of practical shape, and yaw and sweepback should be included. It is important that future results yield the range of strut and flow parameters where the two-dimensional drag prediction holds. Outside of that domain, it may be possible to predict drag on the basis of a three-dimensional flow analysis; such an analysis has been initiated in this report. With respect to the prediction of the flow states, which is particularly important because of the cavity seal-off problem, we suggest in Section 5 that experimental results be examined and the scheme used in this report be again applied. The three-dimensional theoretical analysis of the cavity shape can, after further development, possibly contribute to these matters.

REFERENCES

[1] Perry, B., "Experiments on Struts Piercing the Water Surface", Hydrodynamics Laboratory, California Institute of Technology, Rep. No. E-55.1, Dec. 1954.

[2] Hay, A.D., "Flow about Semi-Submerged Cylinders of Finite Length", Princeton University, Job Order No. 5, Contract No. NObs-34006, October 1, 1947.

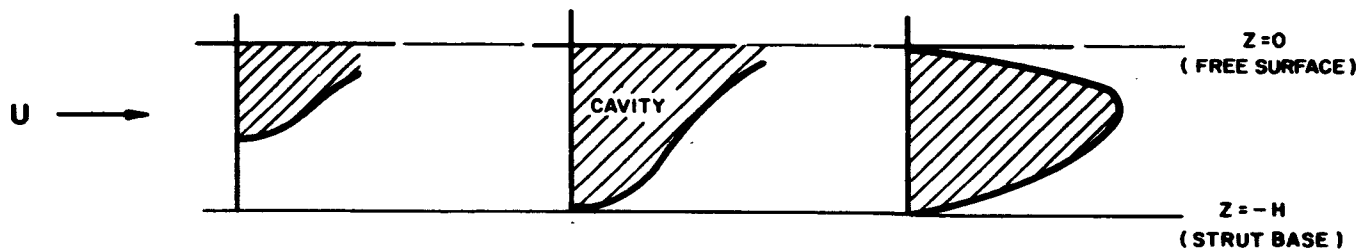

FIG. 3: FLOW STATES

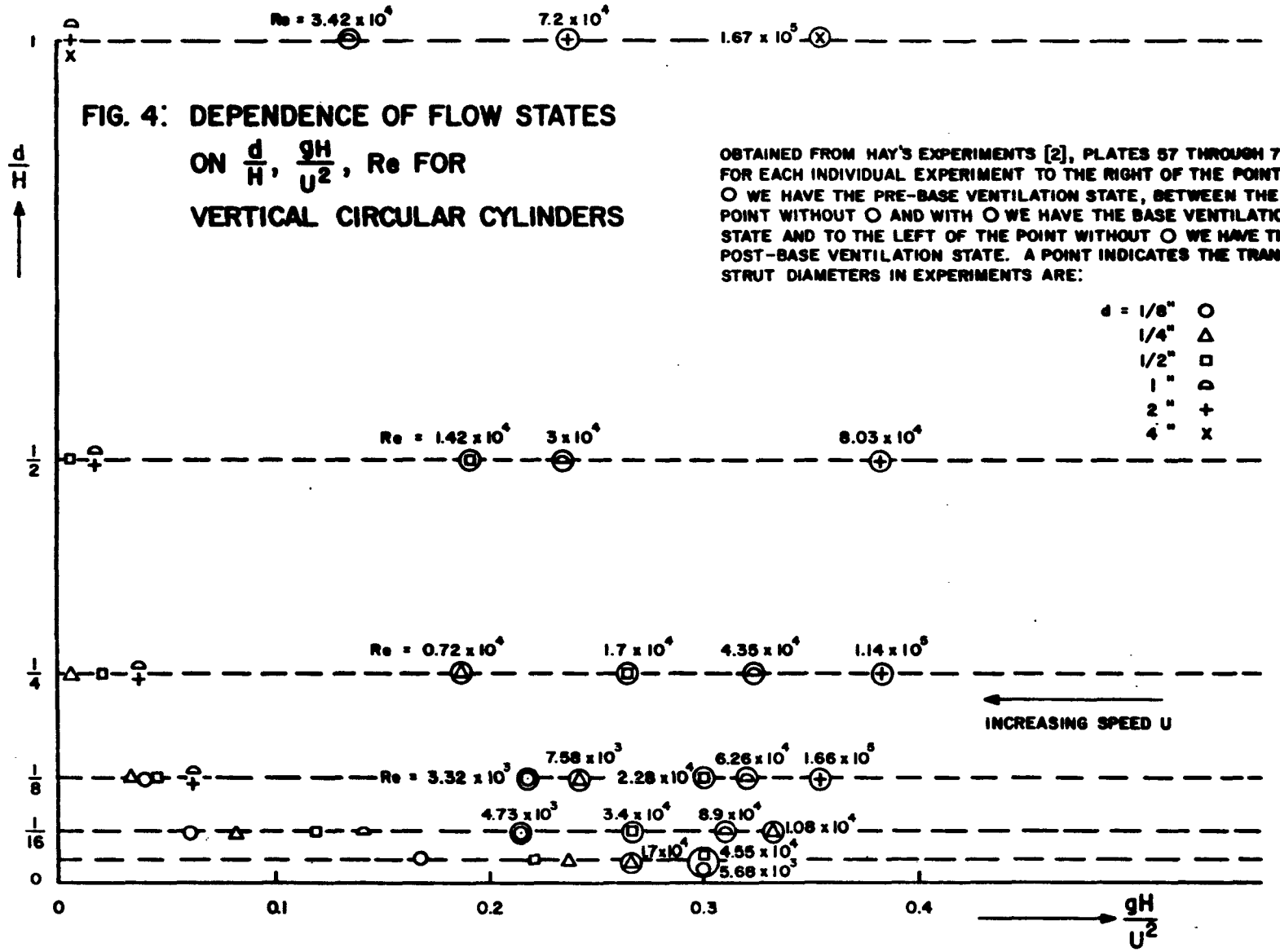

FIG. 4: DEPENDENCE OF FLOW STATES ON $\frac{d}{H}$, $\frac{gH}{U^2}$, Re FOR VERTICAL CIRCULAR CYLINDERS

OBTAINED FROM HAY'S EXPERIMENTS [2], PLATES 57 THROUGH 78. FOR EACH INDIVIDUAL EXPERIMENT TO THE RIGHT OF THE POINT IN O WE HAVE THE PRE-BASE VENTILATION STATE, BETWEEN THE POINT WITHOUT O AND WITH O WE HAVE THE BASE VENTILATION STATE AND TO THE LEFT OF THE POINT WITHOUT O WE HAVE THE POST-BASE VENTILATION STATE. A POINT INDICATES THE TRANSITION. STRUT DIAMETERS IN EXPERIMENTS ARE:

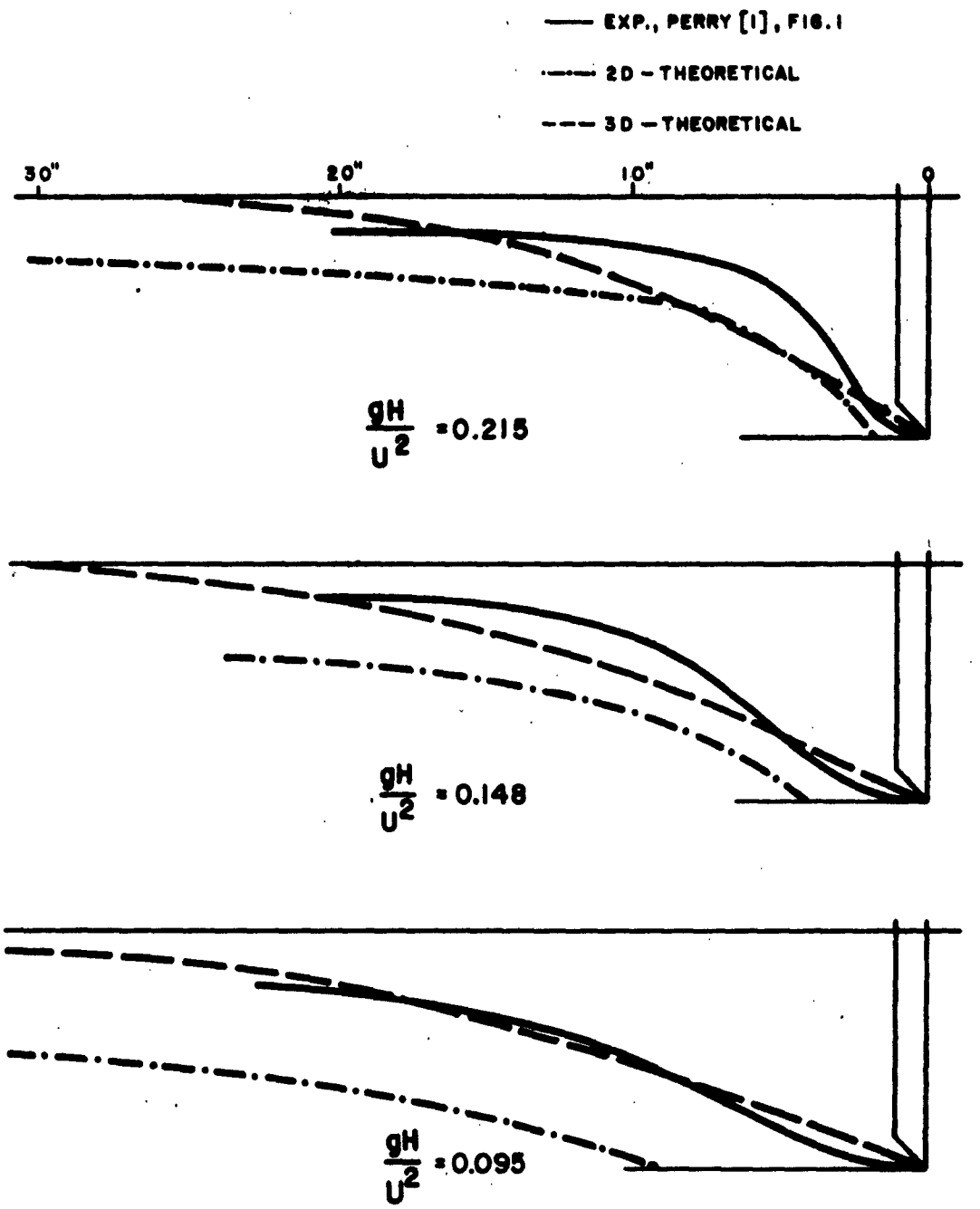

FIG. 5: THEORETICAL AND EXPERIMENTAL VALUES OF CAVITY LENGTHS FOR $\frac{d}{H} = \frac{1}{64}$, $\frac{gH}{U^2}$ = VARIABLE

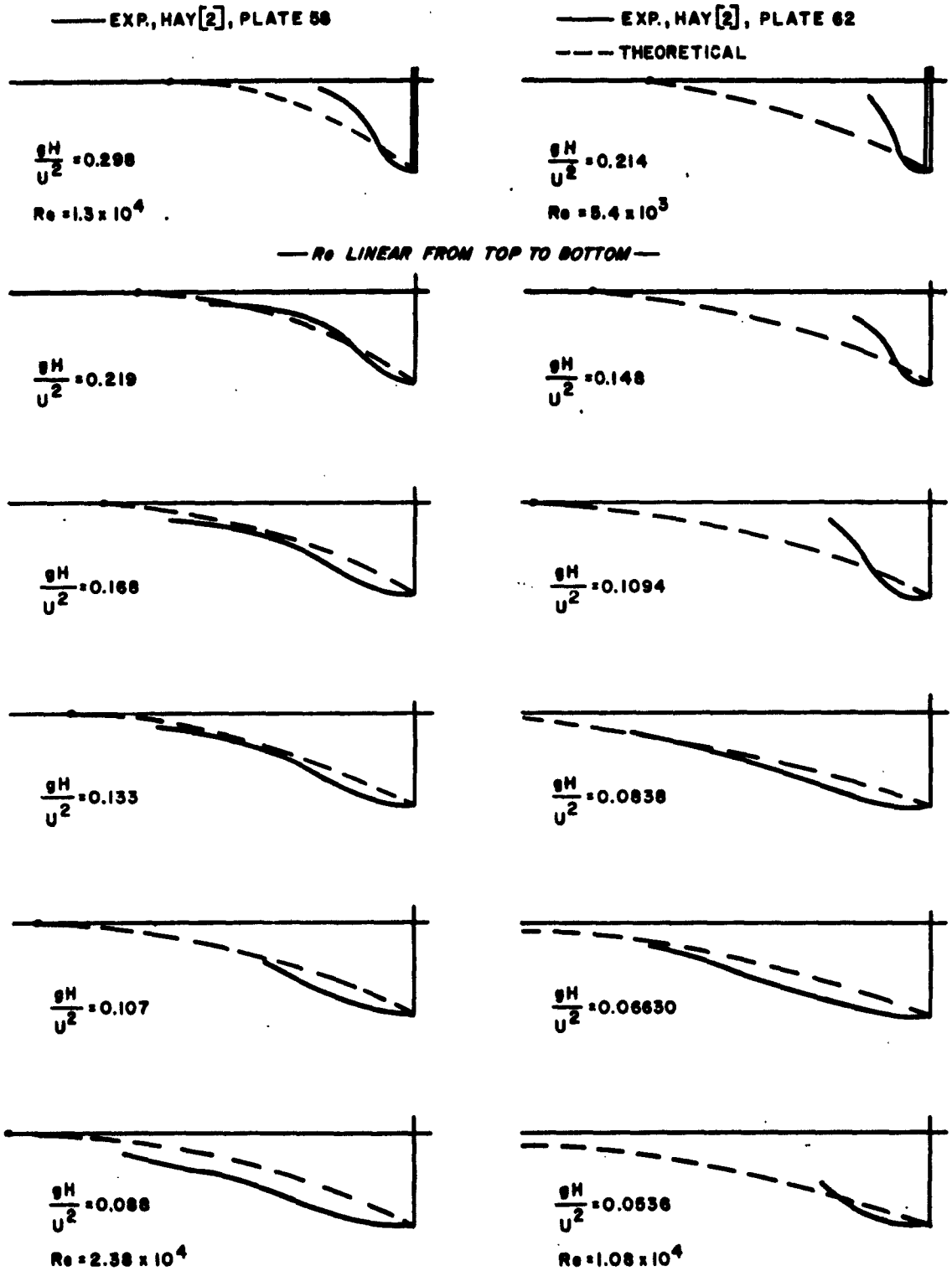

FIG. 6:

FIG. 7:

THEORETICAL AND EXPERIMENTAL VALUES OF CAVITY LENGTHS FOR $\frac{d}{H} = \frac{1}{16}$, $\frac{gH}{U^2}$ = VARIABLE

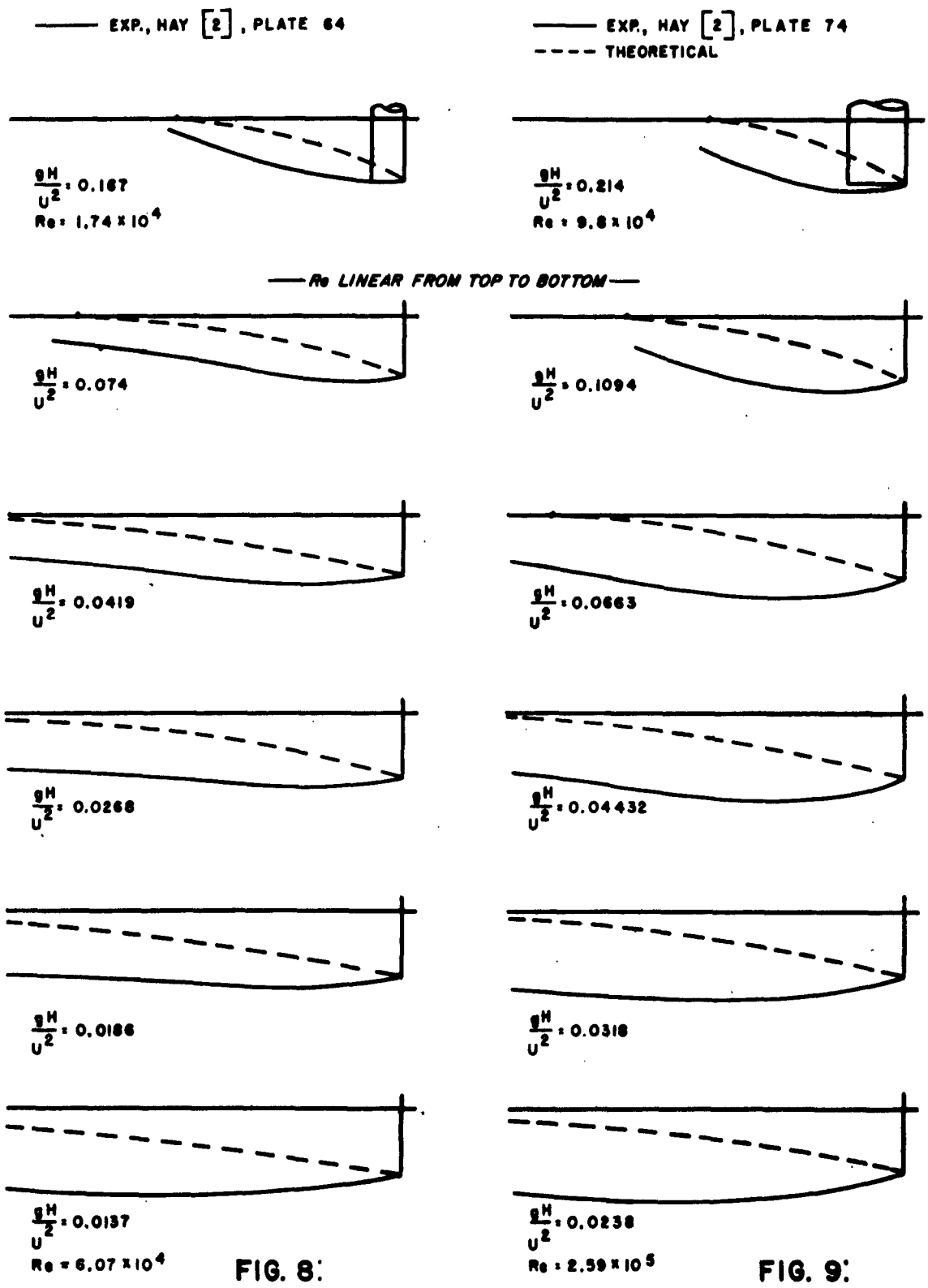

FIG. 8.

FIG. 9.

THEORETICAL AND EXPERIMENTAL VALUES OF CAVITY LENGTHS FOR $\frac{gH}{U^2}$ = VARIABLE, $\frac{d}{H} = \frac{1}{2}$ (IN FIG. 8), $\frac{d}{H} = 1$ (IN FIG. 9)

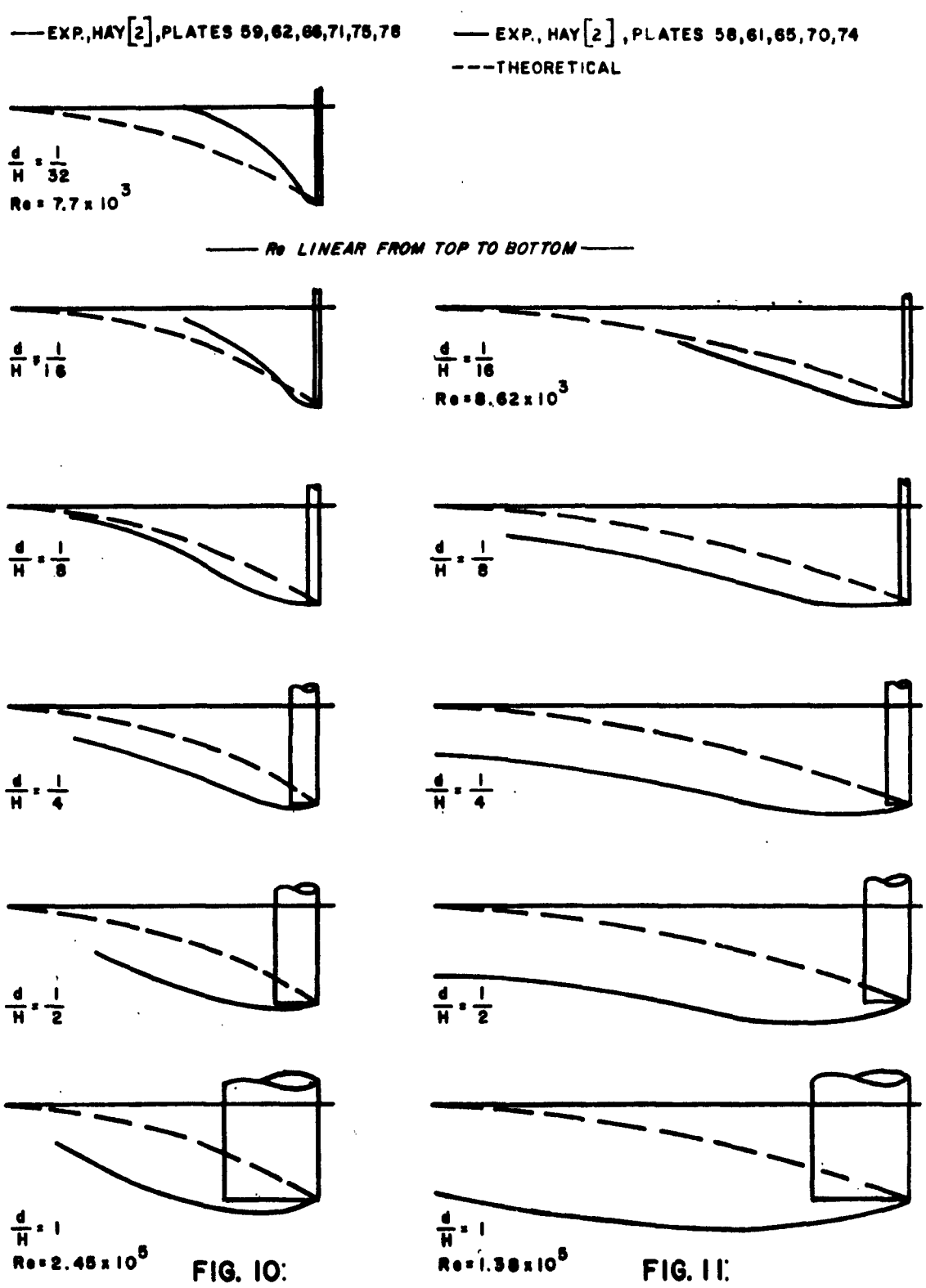

FIG. 10: FIG. 11:

THEORETICAL AND EXPERIMENTAL VALUES OF CAVITY LENGTHS FOR $\frac{d}{H}$ = VARIABLE, $\frac{gH}{U^2}$ = 0.2188 (IN FIG. 10), $\frac{gH}{U^2}$ = 0.084 (IN FIG. 11)

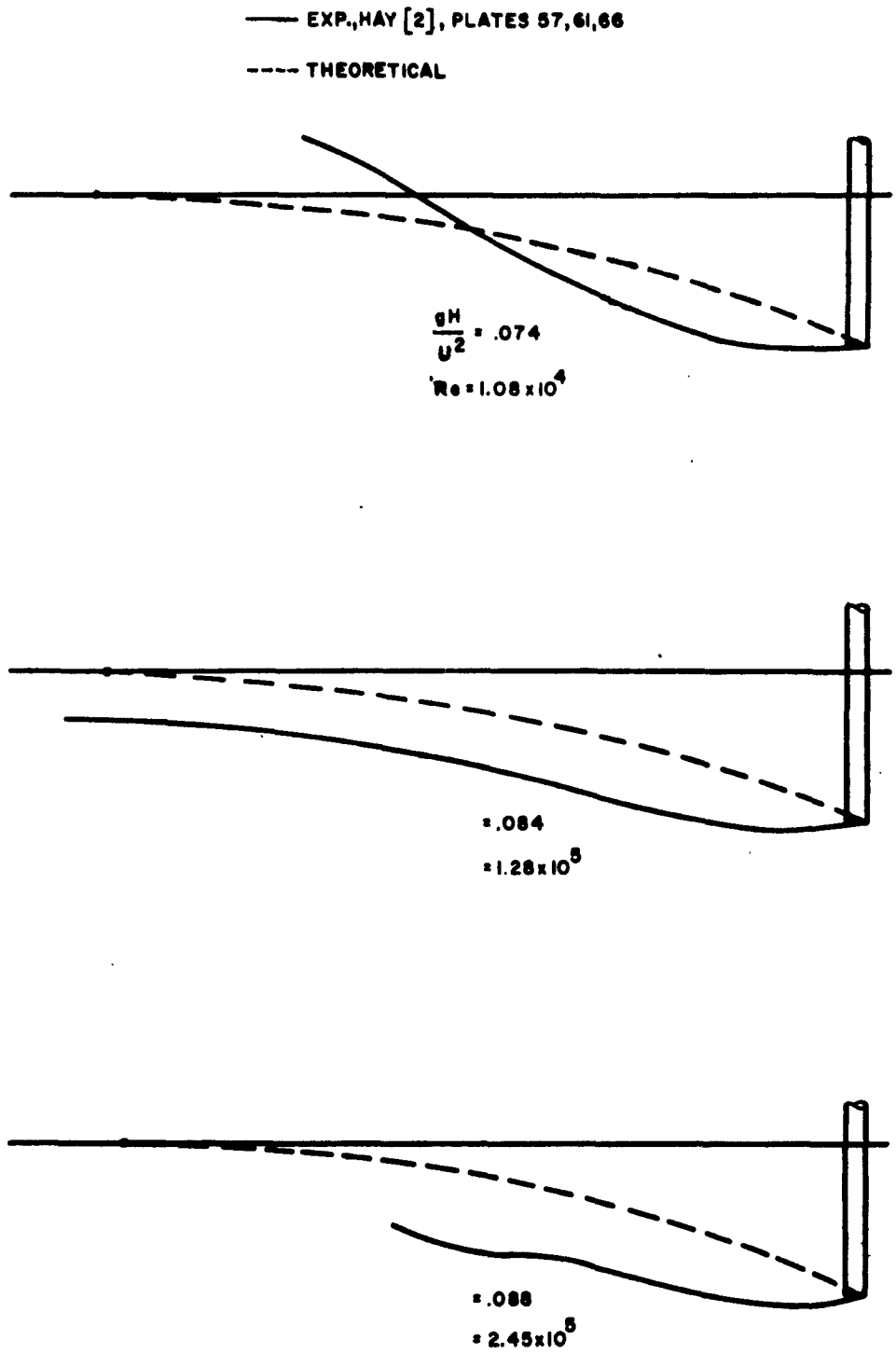

FIG. 12: THEORETICAL AND EXPERIMENTAL VALUES OF CAVITY LENGTHS FOR $\frac{d}{H} = \frac{1}{8}$ = CONST., $\frac{gH}{U^2} \approx 0.084$ = CONST., Re = VARIABLE

FIG 13. THEORETICAL AND EXPERIMENTAL VALUES OF DRAG ON VERTICAL CYLINDER FOR $d = \frac{1}{4}$", H = 1", H = 2"

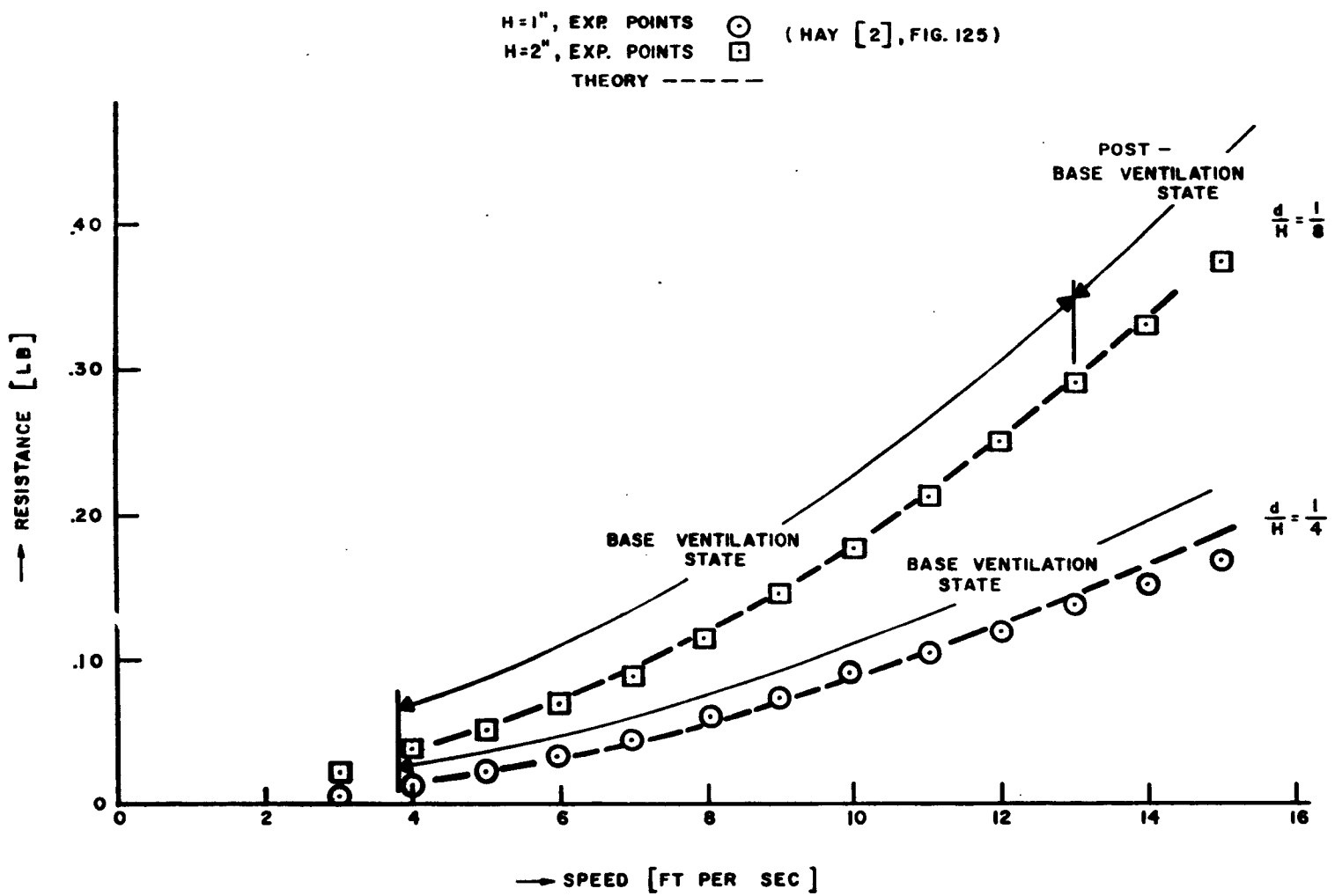

FIG. 14: THEORETICAL AND EXPERIMENTAL VALUES OF DRAG ON VERTICAL CYLINDER FOR $d = \frac{1}{4}$", H = 4"

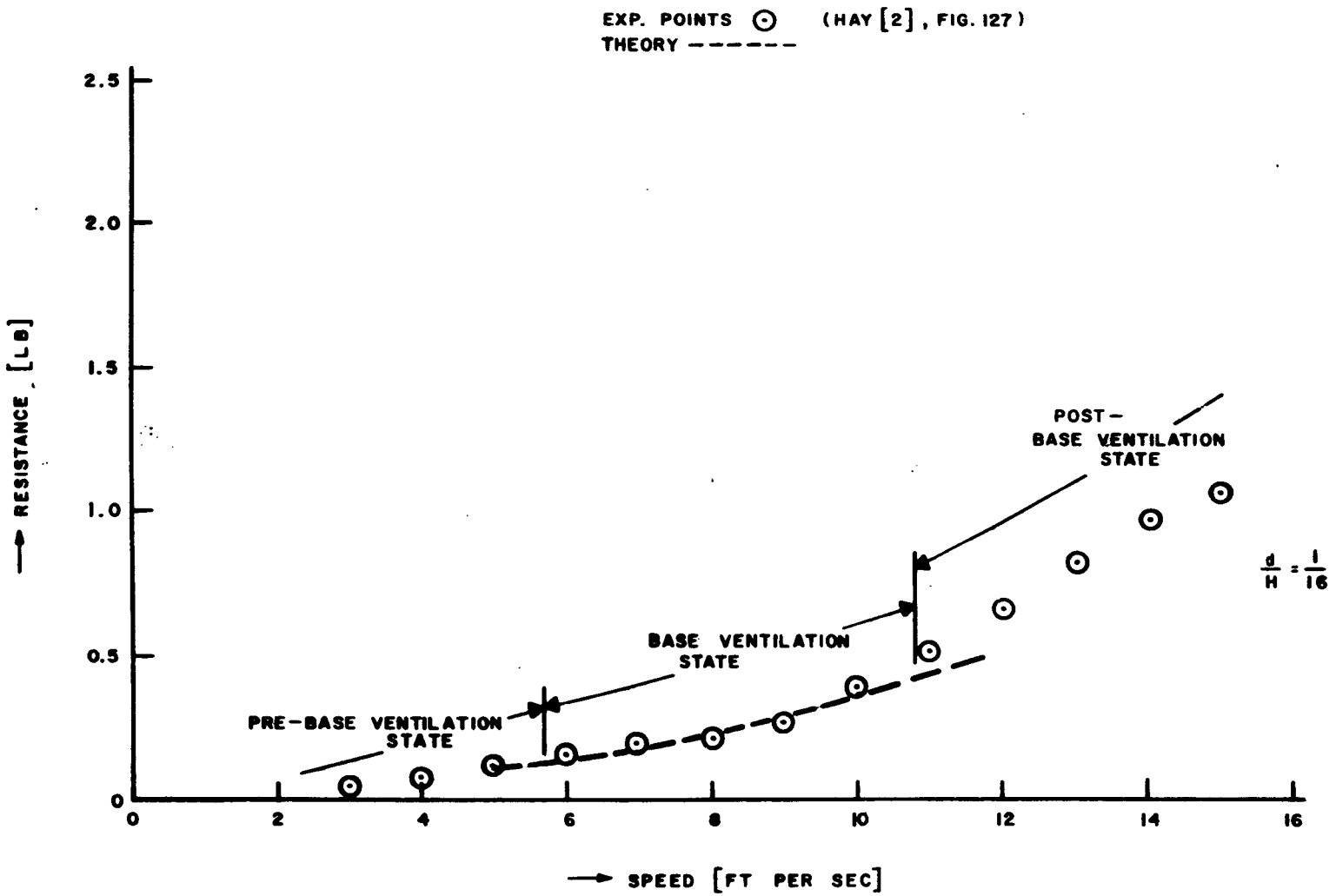

FIG. 15: THEORETICAL AND EXPERIMENTAL VALUES OF DRAG ON VERTICAL CYLINDER FOR $d = \frac{1}{2}$", H = 2", H = 4"

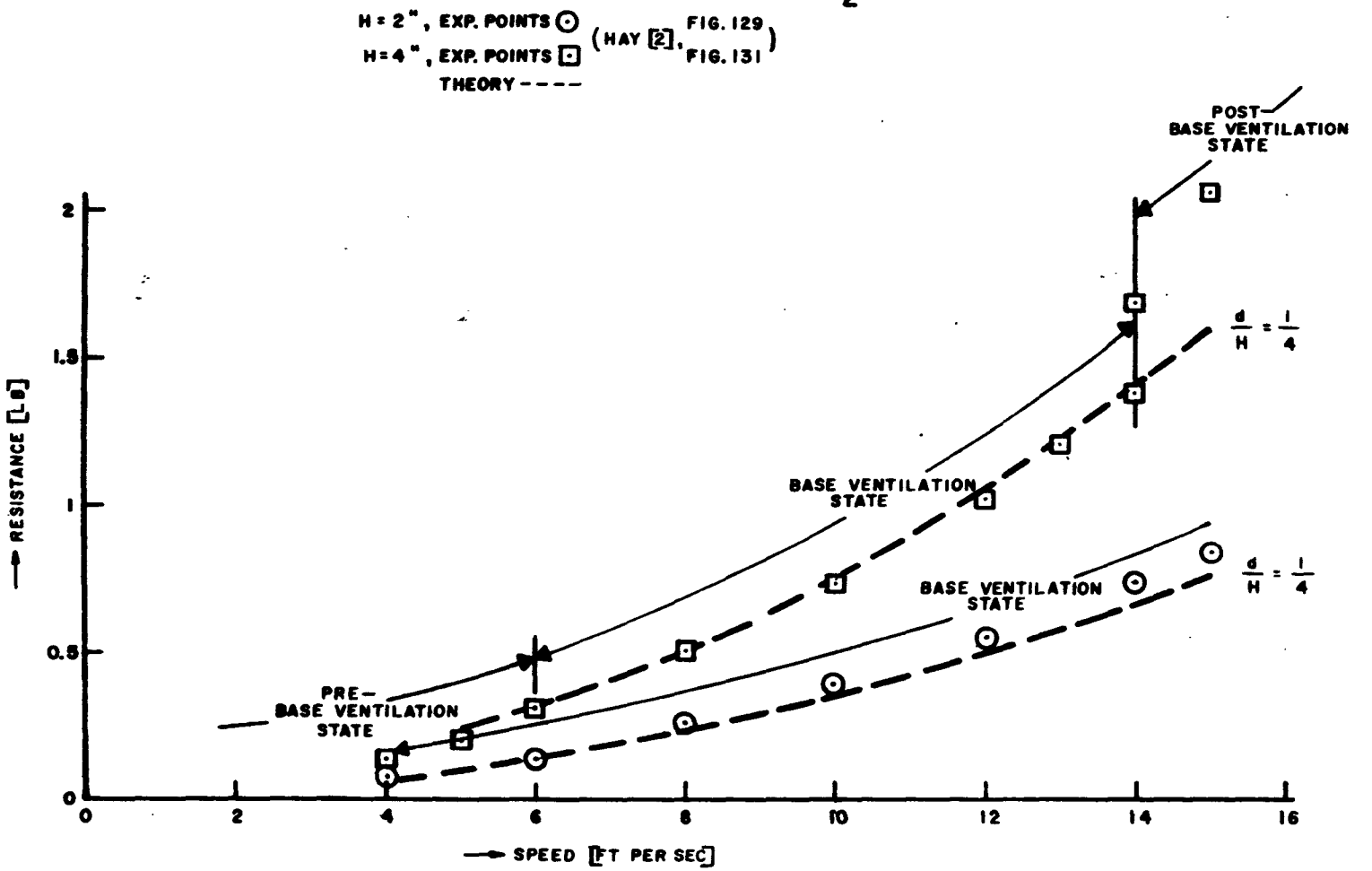

FIG. 16: THEORETICAL AND EXPERIMENTAL VALUES OF DRAG ON VERTICAL CYLINDER FOR $d = \frac{1}{2}$", H = 8"; d = 1", H = 2"

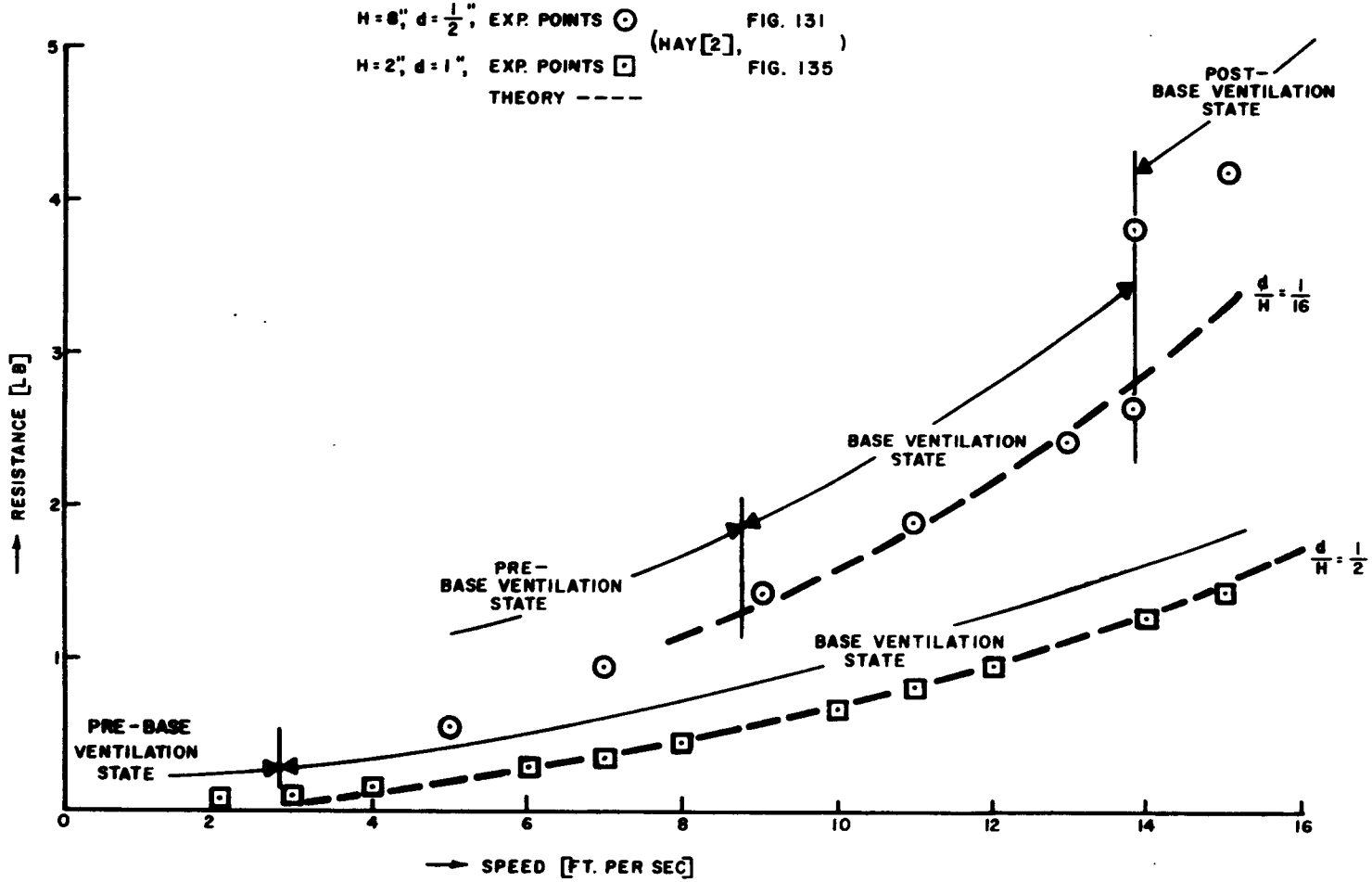

FIG. 17: THEORETICAL AND EXPERIMENTAL VALUES OF DRAG ON VERTICAL CYLINDER FOR d = 1", H = 4", H = 8"

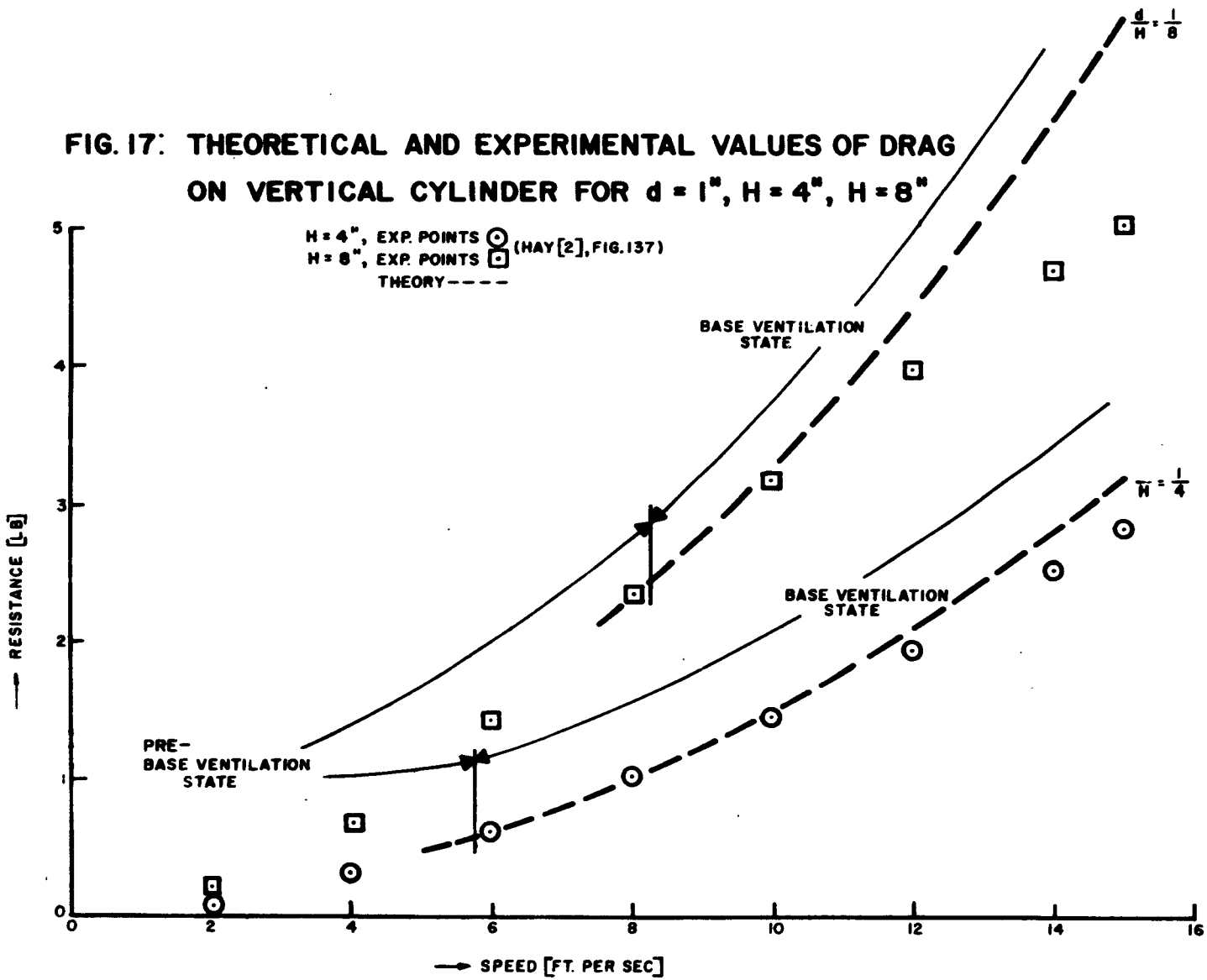

FIG. 18: THEORETICAL AND EXPERIMENTAL VALUES OF DRAG ON VERTICAL CYLINDER FOR d = 1", H = 16"; d = 2", H = 4"

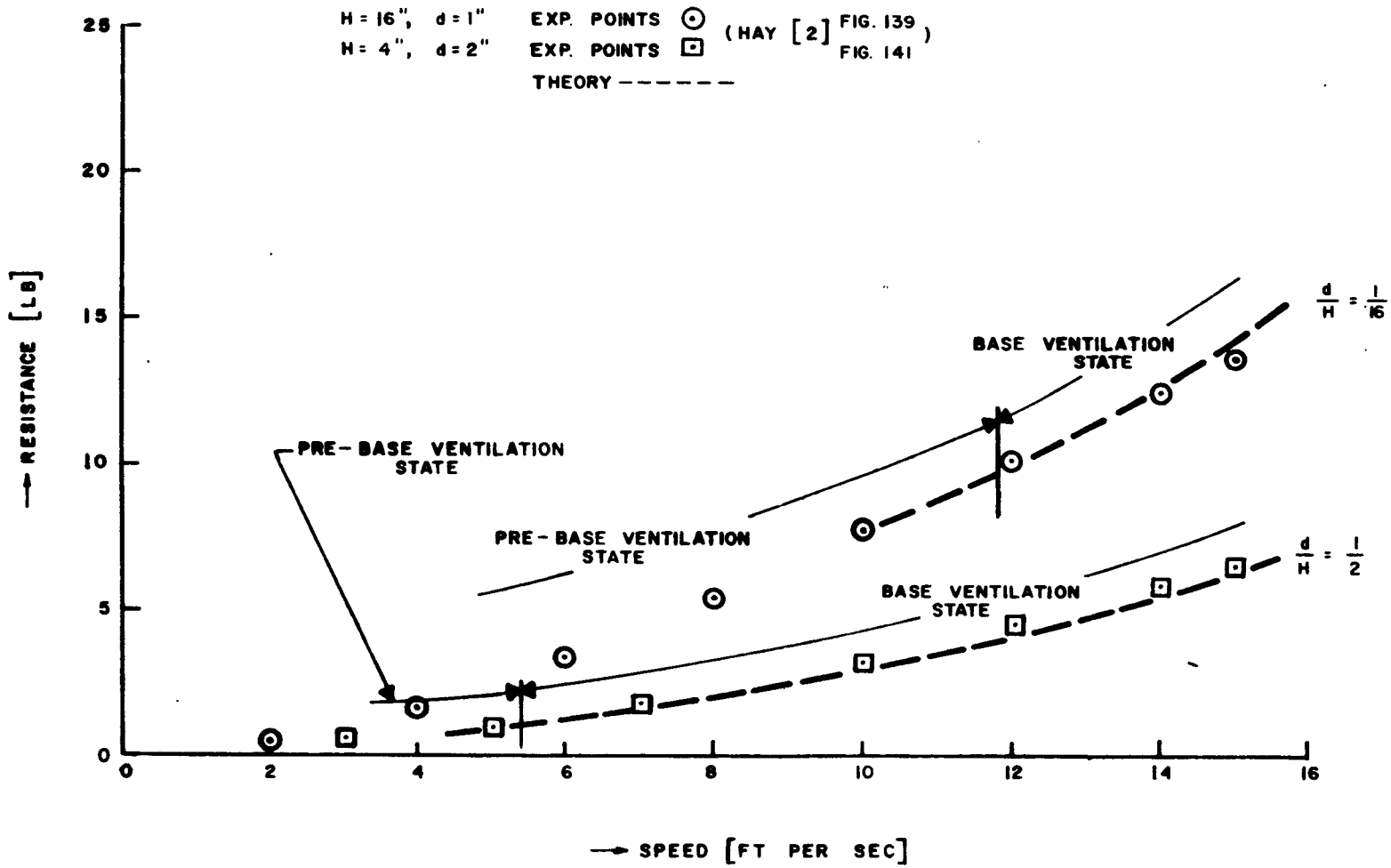

FIG. 19: THEORETICAL AND EXPERIMENTAL VALUES OF DRAG ON VERTICAL CYLINDER FOR d = 2", H = 8", H = 16"

H = 8", EXP. POINTS ●
H = 16", EXP. POINTS ■ (HAY [2], FIG. 143)
THEORY ------

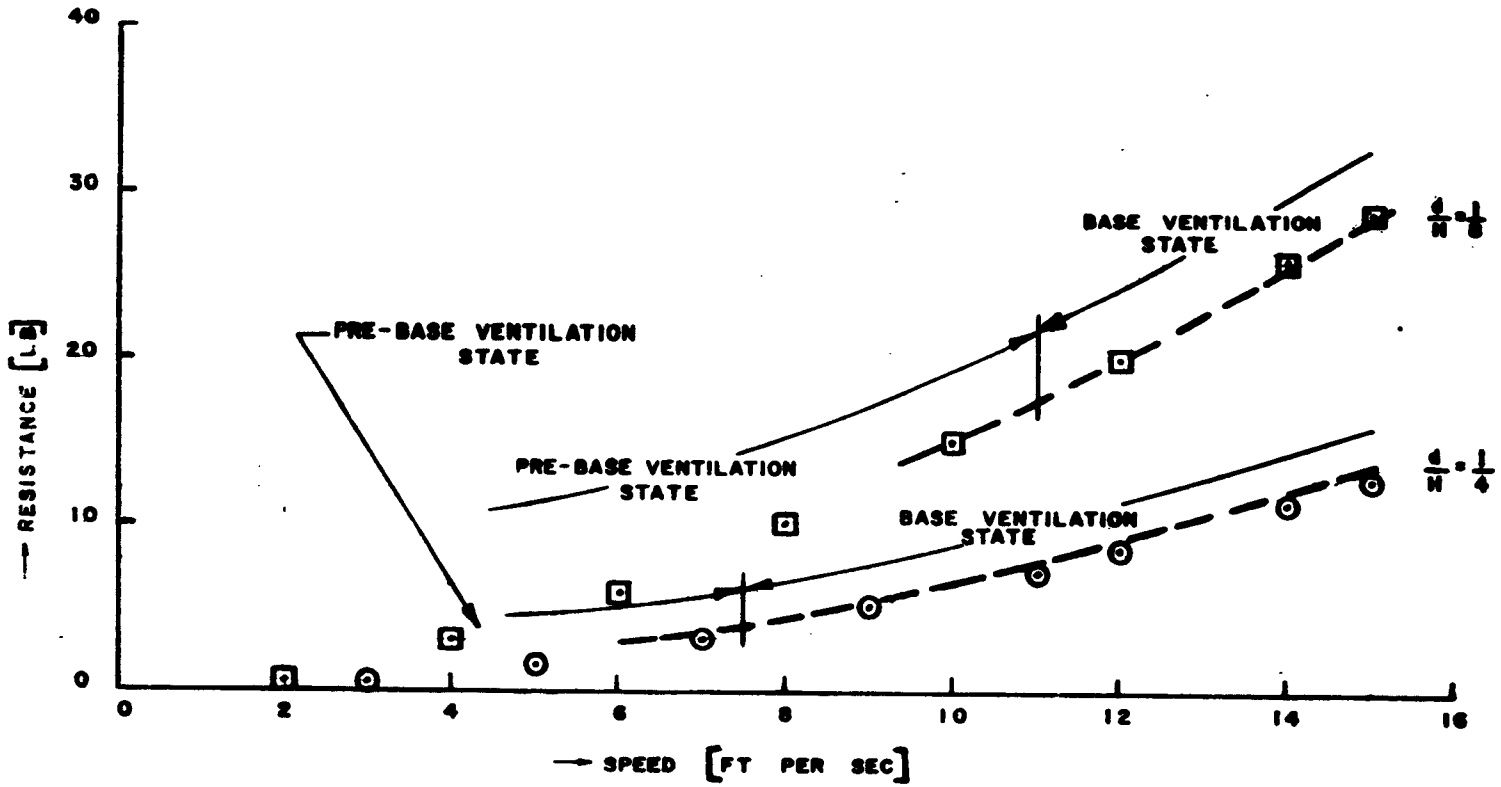

Dr. L. G. Straub, Director
St. Anthony Falls Hydraulic Lab.
University of Minnesota
Minneapolis 14, Minnesota 1
Attn: Mr. J. N. Wetzel 1
Professor B. Silberman 1

Professor J. J. Foody
Engineering Department
New York State University Maritime College
Fort Schulyer, New York 1

New York University
Institute of Mathematical Sciences
25 Waverly Place
New York 3, New York
Attn: Professor J. Keller 1
Professor J. J. Stoker 1

The Johns Hopkins University
Department of Mechanical Engineering
Baltimore 18, Maryland
Attn: Professor S. Corrsin 1
Professor O. M. Phillips 2

Massachusetts Institute of Technology
Department of Naval Architecture and Marine Engineering
Cambridge 39, Massachusetts
Attn: Professor M. A. Abkowitz, Head 1

Dr. G. F. Wislicenus
Ordnance Research Laboratory
Pennsylvania State University
University Park, Pennsylvania 1
Attn: Dr. M. Sevik 1

Professor R. C. DiPrima
Department of Mathematics
Rensselaer Polytechnic Institute
Troy, New York

Stevens Institute of Technology
Davidson Laboratory
Castle Point Station
Hoboken, New Jersey
Attn: Mr. D. Savitsky 1
Mr. J. P. Breslin 1
Mr. C. J. Henry 1
Mr. S. Tsakonas 1

Webb Institute of Naval Architecture
Crescent Beach Road
Glen Cove, New York
Attn: Professor E. V. Lewis 1
Technical Library

Director
Woods Hole Oceanographic Institute
Woods Hole, Massachusetts 1

Executive Director
Air Force Office of Scientific Research
Washington 25, D. C.
Attn: Mechanics Branch 1

Commander
Wright Air Development Division
Aircraft Laboratory
Wright-Patterson Air Force Base, Ohio
Attn: Mr. W. Mykytow, Dynamics Branch 1

Cornell Aeronautical Laboratory
4455 Genesee Street
Buffalo, New York
Attn: Mr. W. Targoff 1
Mr. R. White 1

Massachusetts Institute of Technology
Fluid Dynamics Research Laboratory
Cambridge 39, Massachusetts
Attn: Professor H. Ashley 1
Professor M. Landahl 1
Professor J. Dugundji 1

Hamburgische Schiffbau-Versuchsanstalt
Bramfelder Strasse 164
Hamburg 33, Germany
Attn: Dr. O. Grim 1
Dr. H. W. Lerbs 1

Institut fur Schiffbau der Universitat Hamburg
Berliner Tor 21
Hamburg 1, Germany
Attn: Prof. G. P. Weinblum, Dir. 1

Transportation Technical Research Institute
1-1057, Mejiro-Cho, Toshima-Ku
Tokyo, Japan 1

Max-Planck Institut fur Strömungsforschung
Bottingerstrasse 6/8
Göttingen, Germany
Attn: Dr. H. Reichardt 1

Hydro-og Aerodynamisk Laboratorium
Lyngby, Denmark
Attn: Professor Carl Prohaska 1

Skipsmodelltanken
Trondheim, Norway
Attn: Professor J. K. Lunde 1

Versuchsanstalt fur Wasserbau und Schiffbau
Schleuseninsel im Tiergarten
Berlin, Germany
Attn: Dr. S. Schuster, Director 1
Dr. H. Schwanecke 1
Dr. Grosse 1

Technische Hogeschool
Institut voor Toegepaste Wiskunde
Julianalaan 132
Delft, Netherlands
Attn: Professor R. Timman 1

Bureau D'Analyse et de Recherche Appliquees
47 Avenue Victor Cresson
Issy-Les-Moulineaux
Seine, France
Attn: Professor Siestrunck 1

Netherlands Ship Model Basin
Wageningen, The Netherlands
Attn: Dr. Ir. J. D. van Manen 1

National Physical Laboratory
Teddington, Middlesex, England
Attn: Mr. A. Silverleaf, Superintendent Ship Division 1
Head, Aerodynamics Division 1

Head, Aerodynamics Department
Royal Aircraft Establishment
Farnborough, Hants, England
Attn: Mr. M. O. W. Wolfe 2

Dr. S. F. Hoerner
148 Busteed Drive
Midland Park, New Jersey 1

Boeing Airplane Company
Seattle Division
Seattle, Washington
Attn: Mr. M. J. Turner 1

Electric Boat Division
General Dynamics Corporation
Groton, Connecticut
Attn: Mr. Robert McCandliss 1

General Applied Sciences Labs., Inc.
Merrick and Stewart Avenues
Westbury, Long Island, New York 1

Gibbs and Cox, Inc.
21 West Street
New York, New York 1

Grumman Aircraft Engineering Corp.
Bethpage, Long Island, New York
Attn: Mr. E. Baird 1
Mr. E. Bower 1
Mr. W. P. Carl 1

Lockheed Aircraft Corporation
Missiles and Space Division
Palo Alto, California
Attn: R. W. Kermeen 1

Midwest Research Institute
425 Volker Blvd.
Kansas City 10, Missouri
Attn: Mr. Zeydel 1

Director, Department of Mechanical Sciences
Southwest Research Institute
8500 Culebra Road
San Antonio 6, Texas
Attn: Dr. H. N. Abramson 1
Mr. G. Ransleben 1
Editor, Applied Mechanics Review 1

Convair
A Division of General Dynamics
San Diego, California
Attn: Mr. R. H. Oversmith 1
Mr. H. T. Brooke 1

Hughes Tool Company
Aircraft Division
Culver City, California
Attn: Mr. M. S. Harned 1

Hydronautics, Incorporated
Pindell School Road
Howard County
Laurel, Maryland
Attn: Mr. Phillip Eisenberg 1

Rand Development Corporation
13600 Deise Avenue
Cleveland 10, Ohio
Attn: Dr. A. S. Iberall 1

U.S. Rubber Company
Research and Development Department
Wayne, New Jersey
Attn: Mr. L. M. White 1

Technical Research Group, Inc.
2 Aerial Way
Syosset, Long Island, New York
Attn: Mr. Jack Kotik 1

Mr. C. Wigley
Flat 102
6-9 Charterhouse Square
London, E.C. 1, England 1

AVCO Corporation
Lycoming Division
1701 K Street, N.W.
Apt. No. 904
Washington, D. C.
Attn: Mr. T. A. Duncan 1

Mr. J. G. Baker
Baker Manufacturing Company
Evansville, Wisconsin 1

Curtiss-Wright Corporation Research Division
Turbomachinery Division
Quehanna, Pennsylvania
Attn: Mr. George H. Pedersen 1

Dr. Blaine R. Parkin
AiResearch Manufacturing Corporation
9851-9951 Sepulveda Boulevard
Los Angeles 45, California 1

The Boeing Company
Aero-Space Division
Seattle 24, Washington
Attn: Mr. R. E. Bateman 1
(Internal Mail Station 46-74)

Lockheed Aircraft Corporation
California Division
Hydrodynamics Research
Burbank, California
Attn: Mr. Bill East 1

National Research Council
Montreal Road
Ottawa 2, Canada
Attn: Mr. E. S. Turner 1

The Rand Corporation
1700 Main Street
Santa Monica, California
Attn: Technical Library 1

Stanford University
Department of Civil Engineering
Stanford, California
Attn: Dr. Byrne Perry 1
Dr. E. Y. Hsu 1

Dr. Hirsh Cohen
IBM Research Center
P.O. Box 218
Yorktown Heights, New York 1

Mr. David Wellinger
Hydrofoil Projects
Radio Corporation of America
Burlington, Massachusetts 1

Food Machinery Corporation
P.O. Box 367
San Jose, California
Attn: Mr. G. Tedrew 1

Dr. T. R. Goodman
Oceanics, Inc.
Technical Industrial Park
Plainview, Long Island, New York 1

Professor Brunelle
Department of Aeronautical Engineering
Princeton University
Princeton, New Jersey 1

Commanding Officer
Office of Naval Research Branch Office
86 East Randolph Street
Chicago 1, Illinois 1

Commanding Officer and Director
U.S. Navy Mine Defense Laboratory
Panama City, Florida 1

Commanding Officer
NROTC and Naval Administrative Unit
Massachusetts Institute of Technology
Cambridge 39, Massachusetts 1

U.S. Army Transportation Research and Development Command
Fort Eustis, Virginia
Attn: Marine Transport Division 1

Mr. J. B. Parkinson
National Aeronautics and Space Administration
1512 H Street, N.W.
Washington 25, D.C. 1

Director
Langley Research Center
Langley Station
Hampton, Virginia
Attn: Mr. I. E. Garrick 1
Mr. D. J. Marten 1

Director Engineering Sciences Division
National Science Foundation
1951 Constitution Avenue, N.W.
Washington 25, D.C. 1

Director
National Bureau of Standards
Washington 25, D.C.
Attn: (Fluid Mechanics Division)
(Dr. G. B. Schubauer) 1
Dr. G. H. Keulegan 1
Dr. J. M. Franklin 1

Armed Services Technical Information Agency
Arlington Hall Station
Arlington 12, Virginia 10

Office of Technical Services
Department of Commerce
Washington 25, D.C. 1

California Institute of Technology
Pasadena 4, California
Attn: Professor M. S. Plesset 1
Professor T. Y. Wu 1
Professor A. J. Acosta 1

University of California
Department of Engineering
Los Angeles 24, California
Attn: Dr. A. Powell 1

Director
Scripps Institute of Oceanography
University of California
La Jolla, California 1

Professor M. L. Albertson
Department of Civil Engineering
Colorado A&M College
Fort Collins, Colorado 1

Professor J. E. Cermak
Department of Civil Engineering
Colorado State University
Fort Collins, Colorado 1

Professor W. R. Sears
Graduate School of Aeronautical Engineering
Cornell University
Ithaca, New York 1

State University of Iowa
Iowa Institute of Hydraulic Research
Iowa City, Iowa
Attn: Dr. H. Rouse 1
Dr. L. Landweber 1

Harvard University
Cambridge 38, Massachusetts
Attn: Professor G. Birkhoff
(Dept. of Mathematics) 1
Professor G. F. Carrier
(Dept. of Mathematics) 1

Massachusetts Institute of Technology
Cambridge 39, Massachusetts
Attn: Department of Naval Architecture and Marine Engineering
Professor A. T. Ippen 1

University of Michigan
Ann Arbor, Michigan
Attn: Professor R. B. Couch
(Dept. of Naval Architecture) 1
Professor W. W. Willmarth
(Aero. Engrg. Department) 1
Professor M. S. Uberoi
(Aero. Engrg. Department) 1

Chief of Naval Research
Department of the Navy
Washington 25, D. C.
Attn: Codes 438 3
461 1
463 1
466 1

Commanding Officer
Office of Naval Research
Branch Office
495 Summer Street
Boston 10, Massachusetts 1

Commanding Officer
Office of Naval Research
Branch Office
207 West 24th Street
New York 11, New York 1

Commanding Officer
Office of Naval Research
Branch Office
1030 East Green Street
Pasadena, California 1

Commanding Officer
Office of Naval Research
Branch Office
1000 Geary Street
San Francisco 9, Calif. 1

Commanding Officer
Office of Naval Research
Branch Office
Box 39, Navy No. 100
Fleet Post Office
New York, New York 25

Director
Naval Research Laboratory
Washington 25, D.C.
Attn: Code 2027 6

Chief, Bureau of Naval Weapons
Department of the Navy
Washington 25, D. C.
Attn: Codes RUAW-4 1
RRRE 1
RAAD 1
RAAD-222 1
DIS-42 1

Chief, Bureau of Ships
Department of the Navy
Washington 25, D. C.
Attn: Codes 310 1
312 1
335 1
420 1
421 1
440 1
442 1
449 1

Chief, Bureau of Yards and Docks
Department of the Navy
Washington 25, D. C.
Attn: Code D-400 1

Commanding Officer and Director
David Taylor Model Basin
Washington 7, D. C.
Attn: Codes 108 1
142 1
500 1
513 1
520 1
525 1
526 1
526A 1
530 1
533 1
580 1
585 1
589 1
591 1
591A 1
700 1

Commander
U.S. Naval Ordnance Test Station
China Lake, California
Attn: Code 753 1

Commander
U.S. Naval Ordnance Test Station
Pasadena Annex
3202 E. Foothill Blvd.
Pasadena 8, California 1
Attn: Code P-508 1

Commander
Planning Department
Portsmouth Naval Shipyard
Portsmouth, New Hampshire 1

Commander
Planning Department
Boston Naval Shipyard
Boston 29, Massachusetts 1

Commander
Planning Department
Pearl Harbor Naval Shipyard
Navy No. 128, Fleet Post Office
San Francisco, California

Commander
Planning Department
San Francisco Naval Shipyard
San Francisco 24, California 1

Commander
Planning Department
Mare Island Naval Shipyard
Vallejo, California 1

Commander
Planning Department
New York Naval Shipyard
Brooklyn 1, New York 1

Commander
Planning Department
Puget Sound Naval Shipyard
Bremerton, Washington 1

Commander
Planning Department
Philadelphia Naval Shipyard
U.S. Naval Base
Philadelphia 12, Pa. 1

Commander
Planning Department
Norfolk Naval Shipyard
Portsmouth, Virginia 1

Commander
Planning Department
Charleston Naval Shipyard
U.S. Naval Base
Charleston, South Carolina 1

Commander
Planning Department
Long Beach Naval Shipyard
Long Beach 2, California 1

Commander
Planning Department
U.S. Naval Weapons Laboratory
Dahlgren, Virginia 1

Commander
U.S. Naval Ordnance Laboratory
White Oak, Maryland 1

Dr. A. V. Hershey
Computation and Exterior
Ballistics Laboratory
U.S. Naval Weapons Laboratory
Dahlgren, Virginia 1

Superintendent
U.S. Naval Academy
Annapolis, Maryland
Attn: Library 1

Superintendent
U.S. Naval Postgraduate School
Monterey, California 1

Commandant
U.S. Coast Guard
1300 E. Street, N.W.
Washington, D. C. 1

Secretary Ship Structure Committee
U.S. Coast Guard Headquarters
1300 E. Street, N.W.
Washington, D.C. 1

Commander
Military Sea Transportation Service
Department of the Navy
Washington 25, D.C.

U.S. Maritime Administration
GAO Building
441 G Street, N.W.
Washington, D. C.
Attn: Division of Ship Design 1
Division of Research 1

Superintendent
U.S. Merchant Marine Academy
Kings Point, Long Island, New York
Attn: Capt. L. S. McCready (Dept.
of Engineering) 1